Research Square

Preprints are preliminary reports that have not undergone peer review.
They should not be considered conclusive, used to inform clinical practice,
or referenced by the media as validated information.

Muted Tropical Pacific Ocean Carbon Response to the 2023 Extreme El Niño

Enhui Liao

ehliao@sjtu.edu.cn

Shanghai Jiao Tong University https://orcid.org/0000-0002-5516-7831

Weixian Zeng

Shanghai Jiao Tong University

Xueying Zhang

Baoxiao Qu

Institute of Oceanology, Chinese Academy of Sciences

Xueming Zhu

Guansuo Wang

Shiyu Liang

Shanghai Jiao Tong University https://orcid.org/0009-0003-2917-2033

Alizée Roobaert

Jens Müller

ETH Zurich https://orcid.org/0000-0003-3137-0883

Cong Guan

Article

Keywords:

Posted Date: November 12th, 2026

DOI: https://doi.org/10.21203/rs.3.rs-11226380/v1

License: This work is licensed under a Creative Commons Attribution 4.0 International License.
Read Full License

Additional Declarations: There is **NO** Competing Interest.

Muted tropical Pacific Ocean carbon response to the 2023 extreme El Niño

Abstract

El Niño dominates the interannual variability of global air–sea CO_2 fluxes by suppressing CO_2 outgassing in the tropical Pacific. Using an ensemble of observation-based fCO_2 products and global ocean biogeochemical models (GOBMs), we find that the 2023 El Niño produced an anomalously weak carbon-cycle response. CO_2 outgassing was reduced by only about 0.1 Pg C yr^{-1}, roughly half of the 0.18 Pg C yr^{-1} reduction expected from the historical SST–carbon relationship established during the extreme 1997–1998 and 2015–2016 El Niño events (hereafter 1997/2015). We show that although warming in 2023 was similarly strong, the westerly wind anomaly and upwelling reduction were not as strong as during the previous extreme El Niño events. Consequently, the non-thermal ocean pCO_2 decrease was smaller than in 1997/2015, while the thermal anomaly remained comparable, limiting the net pCO_2 response. In addition, the comparably high wind speeds facilitated high gas-exchange rates, which further prevented the suppression of CO_2 outgassing. These findings highlight the variability and complexity of the canonical El Niño–carbon coupling and call for improved theoretical, modeling, and observational constraints.

1 Introduction

The global ocean absorbs approximately 26% of anthropogenic CO_2 emissions since 1850, thereby slowing the growth of atmospheric CO_2 (Friedlingstein, O'Sullivan, Jones, Andrew, Hauck, et al., 2025). However, the interannual variability of ocean carbon sink remains uncertain in both magnitude and underlying mechanisms (DeVries et al., 2023; Gruber et al., 2023). This variability is dominated by a limited number of highly dynamic regions (Li et al., 2024; M. Zhang et al., 2025), such as the tropical Pacific Ocean, where tightly coupled physical and biogeochemical processes interact nonlinearly (Hauck et al., 2023; Landschützer et al., 2019; Le Quéré et al., 2000; C. Sun et al., 2025). Improving our understanding of the drivers of interannual air–sea CO_2 flux variability is therefore critical for closing the contemporary global carbon budget and for predicting ocean carbon uptake under ongoing climate change (Friedlingstein, O'Sullivan, Jones, Andrew, Hauck, et al., 2025; Mayot et al., 2024).

The tropical Pacific (160°E-285°E, 15°S-15°N) is climatologically the largest natural oceanic source of CO_2 to the atmosphere (0.4–0.5 Pg C yr^{-1}; Ishii et al., 2025) due to equatorial upwelling (Feely et al., 2002; Sutton et al., 2014). During El Niño events, tropical Pacific CO_2 outgassing is typically suppressed by 0.1–0.5 Pg C yr^{-1}, as a result of competing thermal and non-thermal components (Feely et al., 2002; Liao et al., 2020; McKinley et al., 2004). The non-thermal component dominates this reduction by decreasing surface dissolved inorganic carbon (DIC), as weakened upwelling limits subsurface DIC supply and enhanced precipitation dilutes surface waters, thereby lowering oceanic partial pressure of CO_2 (pCO_2) and weakening the air–sea gradient (Ran et al., 2005; Wang et al., 2015; Xiu & Chai, 2014; Parc et al., 2024; Turk et al., 2010). A concurrent decline in biological productivity can

elevate pCO_2 by weakening biological carbon uptake, partially offsetting the ocean pCO_2 suppression (Doney et al., 2009; Dong et al., 2017; Q. Sun & Du, 2025; Vaittinada Ayar et al., 2022; Wong et al., 2022). In contrast, the thermal component plays a secondary role that the ocean surface warming reduces CO_2 solubility, which increases pCO_2 and favours increased CO_2 outgassing (C. Sun et al., 2025; Watanabe et al., 2020; Arteaga et al., 2026).

Historically, stronger El Niño events, as measured by Niño indices (e.g., Niño 3.4), lead to larger reductions in tropical Pacific CO_2 outgassing, which in turn enhances the global ocean carbon sink (Cosca et al., 2003; Feely et al., 2006; Jones et al., 2001). However, the global ocean carbon sink was weakened instead of enhanced during the 2023 El Niño. This reduction has been attributed to marine heatwaves in the subtropical ocean (Müller et al., 2025). Given that the El Niño–Southern Oscillation (ENSO) dominates approximately 70% of the interannual variability in the global air–sea CO_2 flux (Feely et al., 2002; Le Quéré et al., 2000), the suppression of tropical Pacific CO_2 outgassing may also have contributed to the weak global ocean carbon uptake reported for 2023 (Müller et al., 2025). This potential influence motivates further investigation of the mechanisms governing ENSO–carbon coupling during the 2023 event.

The 2023 El Niño was characterized by strong oceanic warming but a relatively weak atmospheric response, with limited anomalies in wind and precipitation (Yang & Li, 2025; Hu et al., 2024; Fan et al., 2026). This is related to the strongly preconditioning by the preceding prolonged La Niña, which built anomalously large subsurface heat content in the western tropical Pacific (Peng et al., 2025; Lian et al., 2023a). As the 2023 El Niño developed, this stored heat was discharged eastward along the equator, producing pronounced sea surface temperature (SST) warming. Meanwhile, concurrent warming in the Atlantic and Indian Oceans amplified the Walker circulation and weakened the Bjerknes feedback over the tropical Pacific, leading to muted wind anomalies, limited thermocline deepening, and only modest suppression of equatorial upwelling (Geng et al., 2024; Kim et al., 2024).

How air–sea CO_2 fluxes responded to the unusual 2023 El Niño remains unclear. This uncertainty is particularly pronounced in the tropical Pacific, where sparse surface ocean pCO_2 observations (Bakker et al., 2016) introduce uncertainties and potential biases in data-driven and machine-learning reconstructions of surface pCO_2 and air–sea CO_2 flux variability (Chau et al., 2022; Gregor & Gruber, 2021; Landschützer et al., 2014). The spread across observation-based fCO_2 products and model estimates over the past decade is markedly larger in the tropical Pacific (0.38 Pg C yr^{-1}) than in the global mean (0.11 Pg C yr^{-1}). A clearer mechanistic understanding of how ocean circulation, upwelling dynamics, and air–sea gas exchange jointly regulate pCO_2 variability will help constrain key drivers of CO_2 flux anomalies and thereby improve the accuracy of observation-based fCO_2 products.

This study quantifies and compares tropical Pacific air–sea CO_2 flux anomalies during the 2023 El Niño and investigates the processes underlying its atypical response. Specifically, we address three questions: (1) how the 2023 CO_2 flux response deviates from the historical SST–carbon coupling, (2) which processes govern the tropical Pacific carbon response under the unique 2023 El Niño dynamics, and (3) the broader implications for understanding ENSO–related carbon variability. We combine nine observation-based fCO_2 products with ten global ocean biogeochemical models (GOBMs) simulations to characterize the muted

tropical carbon response in 2023, and further apply a process-based diagnostic framework using MOM6–COBALT2 outputs to identify the governing mechanisms. This approach enables a mechanistic decomposition of CO_2 flux anomalies into thermal, non-thermal, and gas-transfer contributions, as well as decomposition of non-thermal ocean pCO_2 into transport, biological, precipitation processes.

2 Method

This study employs a global ocean model developed at the Geophysical Fluid Dynamics Laboratory (GFDL) to examine the spatial and temporal variability of air–sea CO_2 fluxes in the tropical Pacific and underlying mechanisms. The modeling system couples the Modular Ocean Model version 6 (MOM6), the Sea Ice Simulator version 2 (SIS2), and the Carbon, Ocean Biogeochemistry, and Lower Trophics model version 2 (COBALT v2), and is hereafter referred to as MOM6-COBALT2 (Adcroft et al., 2019; Stock et al., 2020). A detailed description of the model configuration and external forcing is provided in Section S2 of the Supporting Information.

This model (MOM6-COBALT2) has been comprehensively validated against observational datasets (Figs. S1–S10) and has been widely used in previous ENSO-related ocean carbon cycle studies (C. Sun et al., 2025; Liao et al., 2020; L. Zhang & Liao, 2025). The model successfully reproduces the mean state and interannual variability of key physical and biogeochemical variables in the tropical Pacific, including pCO_2, SST, sea surface salinity (SSS), sea surface height (SSH), DIC, alkalinity, NO_3, PO_4, and chlorophyll (Figs. S1–S10, see details in Section S1). These results demonstrate the model's capability to simulate ENSO-driven carbon variability. Nine observation-based surface ocean fCO_2 reconstructs (fCO_2 products) and ten additional global ocean biogeochemical model (GOBM) simulations compiled and publicly provided by the Global Carbon Project (see details in Section S1; available at https://zenodo.org/records/17579108, Hauck et al. (2025); Friedlingstein, O'Sullivan, Jones, Andrew, Bakker, et al. (2025)), are used to characterize the spatial and temporal variability of air–sea CO_2 flux, evaluate model (MOM6-COBALT2) performance, and examine the relationship between SST and CO_2 flux variability (Figs. S11–S14).

In this study, negative CO_2 flux (FCO_2) indicates oceanic uptake, while positive values indicate outgassing to the atmosphere. To diagnose the physical and biogeochemical processes governing air–sea CO_2 flux variability, the flux anomaly is decomposed into contributions associated with variability in the gas-transfer velocity, variability in the air–sea CO_2 partial pressure difference (ΔpCO_2), and a residual term (Doney et al., 2009). The equation is expressed as:

$$\mathrm{FCO}_2' = \underbrace{K'\Delta(p\mathrm{CO}_2)}_{\mathrm{FCO}_2-\mathrm{GT}} + \underbrace{K\Delta(p\mathrm{CO}_2)'}_{\mathrm{FCO}_2-\Delta p\mathrm{CO}_2} + res \tag{1}$$

In the tropical Pacific, air–sea CO_2 flux variability is usually dominated by the changes in oceanic pCO_2 (Liao et al., 2020), which is attributed to variations in sea surface DIC, total alkalinity (Alk), temperature (T), and salinity (S). A linearized approximation is adopted to relate perturbations in these tracers to changes in oceanic pCO_2 (Takahashi et al., 1993). Among these factors, DIC, alkalinity, and salinity are considered the non-thermal

components, whereas temperature represents the thermal component.

$$\Delta pCO_{2w} \approx \underbrace{\frac{\partial pCO_{2w}}{\partial T}\Delta T}_{pCO_2-T} + \underbrace{\frac{\partial pCO_{2w}}{\partial DIC}\Delta DIC + \frac{\partial pCO_{2w}}{\partial Alk}\Delta Alk + \frac{\partial pCO_{2w}}{\partial S}\Delta S}_{pCO_2-NONT} \tag{2}$$

Variability in each tracer is governed by oceanic processes including horizontal and vertical transport, freshwater fluxes, biological production and remineralization, and air–sea exchange.

To isolate and quantify the contributions of these processes, the temporal tendency of ocean pCO_2 non-thermal component is finally derived and decomposed into six mechanistic components (Liao et al., 2020; Roobaert et al., 2022):

$$\begin{aligned}\underbrace{\left(\partial_t pCO_{2w} - \frac{\partial pCO_{2w}}{\partial DIC}\,DIC_{FCO_2}\right)}_{pCO_2-\text{nonT change}} \approx{}& \underbrace{\left(\frac{\partial pCO_{2w}}{\partial DIC}\,DIC_H + \frac{\partial pCO_{2w}}{\partial Alk}\,Alk_H + \frac{\partial pCO_{2w}}{\partial S}\,S_H\right)}_{H_{circ}} \\ &+ \underbrace{\left(\frac{\partial pCO_{2w}}{\partial DIC}\,DIC_V + \frac{\partial pCO_{2w}}{\partial Alk}\,Alk_V + \frac{\partial pCO_{2w}}{\partial S}\,S_V\right)}_{V_{circ}} \\ &+ \underbrace{\left(\frac{\partial pCO_{2w}}{\partial DIC}\,DIC_{FW} + \frac{\partial pCO_{2w}}{\partial Alk}\,Alk_{FW} + \frac{\partial pCO_{2w}}{\partial S}\,S_{FW}\right)}_{FW} \\ &+ \underbrace{\left(\frac{\partial pCO_{2w}}{\partial DIC}\,DIC_{Bio} + \frac{\partial pCO_{2w}}{\partial Alk}\,Alk_{Bio}\right)}_{Bio}\end{aligned} \tag{3}$$

In the above formulation, H_{circ} represents the horizontal circulation term by accounting for changes in variables (*i.e.* DIC, alkalinity, and salinity) associated with horizontal advection and mixing processes within the surface layer. The vertical circulation term (V_{circ}) quantifies the variability driven by vertical advection and mixing processes, including upwelling, downwelling, and entrainment across the mixing layer. Freshwater forcing (FW) captures modifications arising from precipitation, evaporation, and riverine inputs. Biological effects (Bio) encompass changes associated with biological consumption, organic matter production, and remineralization, as well as calcium carbonate formation and dissolution. Taken together, this decomposition provides a process-based partitioning of ocean pCO_2 variability into physically and biogeochemically interpretable components. The detailed derivation and temporal tendency of the thermal component of oceanic pCO_2 are presented in Section S4 of the Supporting Information.

3 Results

3.1 Muted Tropical Pacific CO_2 Flux Response During the 2023 El Niño

The 2023 El Niño, which peaked during December 2023–February 2024 (DJF 2023/24), exhibits markedly weakened CO_2 and chlorophyll anomalies compared to its strong SST response. During the 2023 event, SST anomalies in the Niño3.4 region reached ~ 1.9°C, comparable to the extreme 1997 and 2015 events (~ 2.2°C; peaking in DJF 1997/98 and DJF 2015/16; Fig. 1a). In contrast, the associated air–sea CO_2 flux anomaly in 2023 (-0.1 ± 0.05 Pg C yr^{-1}) was substantially smaller than observed during the 1997 and 2015

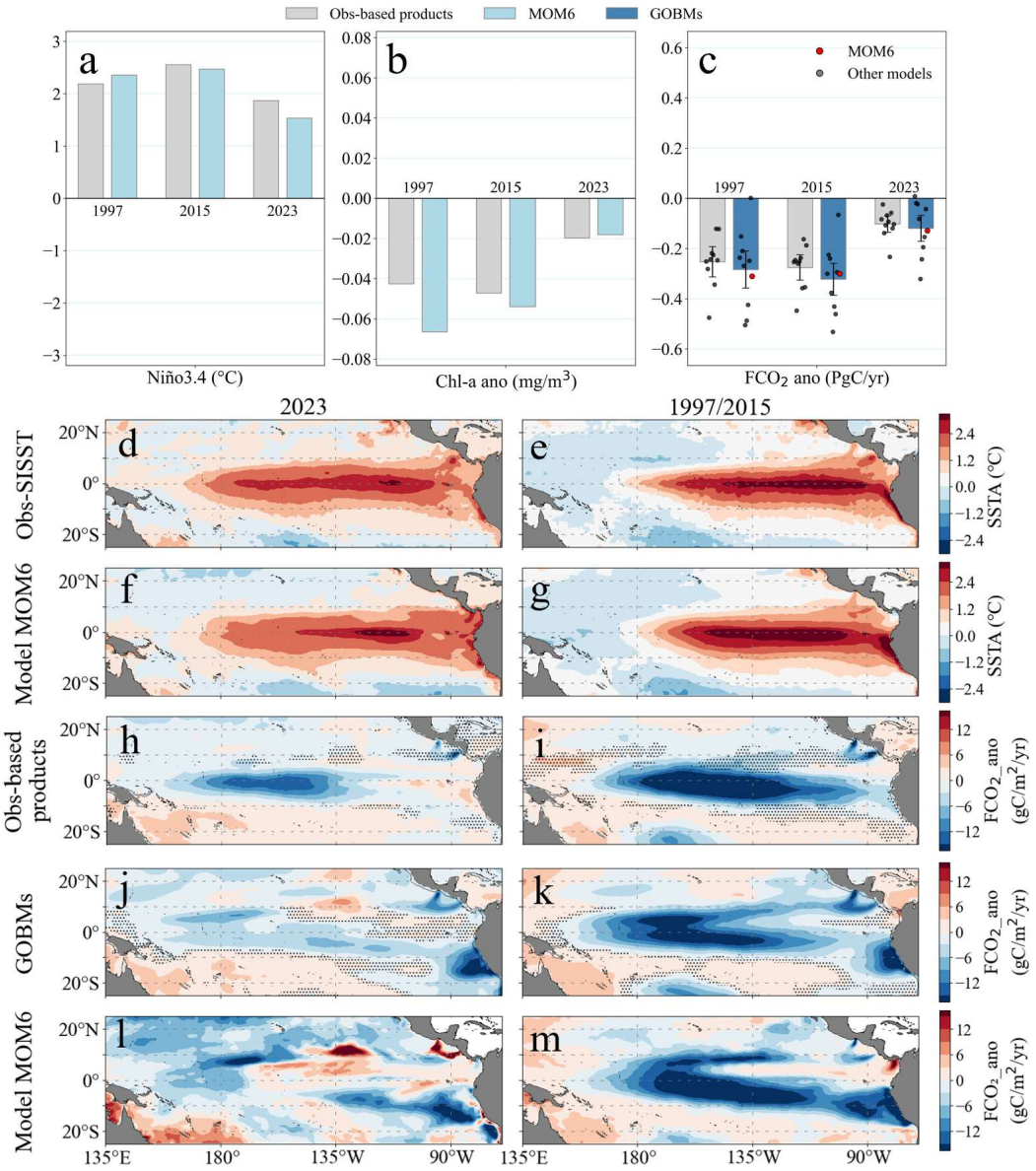


Fig. 1. SST, air–sea CO_2 flux and chlorophyll anomalies during the 2023 extreme El Niño compared with the 1997 and 2015 events. Bar plots (a-c) show SST anomaly in the Niño3.4 region, air–sea CO_2 flux anomaly, and chlorophyll anomaly in the tropical Pacific (160°E–285°E, 15°S–15°N) during major El Niño events. Panels (d–g) display SST anomalies during the 2023 and 1997/2015 events derived from OISST observations and MOM6–COBALT2 simulations. Panels (h–m) show air–sea CO2 flux anomalies for the same events from the ensemble mean of nine observation-based fCO_2 products, ten GOBMs and MOM6–COBALT2 simulations. Bars represent the fCO_2 products/GOBMs ensemble means during the December–February (DJF) of 1997, 2015 and 2023 events, and error bars indicate 95% confidence intervals across datasets. Bar values in panels (a-c) correspond to basin averages over the tropical Pacific based on the DJF mean of monthly anomalies. Spatial anomalies in panels (d–k) are also calculated as the DJF mean of monthly anomalies. Stippling in panels (h-k) indicates regions where the inter-product spread (0.2 standard deviation) exceeds the magnitude of the ensemble-mean anomaly. Dataset details are provided in the Methods and Section S1.

events (-0.27 ± 0.08 Pg C yr^{-1}; Fig. 1c), using the ensemble mean of nine observation-based fCO_2 products.

Based on the historical SST–carbon scaling derived from previous large El Niño events (-0.096 Pg C yr^{-1} per unit Niño3.4 index), the expected 2023 carbon flux anomaly would be approximately -0.18 Pg C yr^{-1}. The observed anomaly (-0.1 ± 0.05 Pg C yr^{-1}) was therefore only about half as large as expected. A similarly muted response is observed in chlorophyll anomalies. While the 1997 and 2015 events produced strong negative chlorophyll anomalies (~ -0.041 to -0.042 mg m^{-3}), the 2023 anomaly (~ -0.02 mg m^{-3}) was likewise only about half as large (Fig. 1b). This attenuated biological response is consistent with the muted carbon signal and further underscores the anomalous biogeochemical behavior of the 2023 event.

The spatial pattern (Figs. 1d–m) indicates that this El Niño carbon breakdown extends across the tropical Pacific at basin scale. SST anomalies in 2023 were comparable in magnitude (2.0 °C) to those in 1997/2015 and exhibited pronounced warming across the central and eastern equatorial Pacific (Figs. 1d–e and S6a–f), although the easternmost warming was less extensive and less intense than during the earlier extreme events. In 1997/2015, the ensemble mean of observation-based fCO_2 products showed that this basin-scale warming coincided with spatially coherent negative anomalies in air–sea CO_2 flux (-12 g C m^{-2} yr^{-1}, Figs. 1i,k,m) and ocean pCO_2 (-16.2 μatm, Figs. S5), forming a continuous band of outgassing suppression across the central and eastern basin.

In contrast, 2023 displayed markedly weaker carbon anomalies (-6 g C m^{-2} yr^{-1} and -5.3 μatm, Figs. 1h,j) that were spatially fragmented, with extensive near-neutral or even opposite-sign signals in the eastern equatorial Pacific. The core region of flux suppression also shifted westward relative to 1997/2015. The GOBM simulations show a similar pattern, with strong reductions in air–sea CO_2 flux during the 1997 and 2015 events but a substantially weaker carbon flux anomaly in 2023. Likewise, the MOM6 model captures both the historical basin-scale SST–carbon coherence and the anomalously weak carbon response observed in 2023 (Figs. 1 and S11–S12).

3.2 Time evolution and decomposition of equatorial Pacific carbon anomalies

The 2023 El Niño stands out as a unique event in the 1982–2024 record, exhibiting a weak tropical Pacific CO_2 flux anomaly despite a high Niño3.4 index. Over previous decades, the ensemble mean of observation-based fCO_2 products showed that pronounced reductions in CO_2 outgassing were consistently associated with stronger Niño3.4 anomalies (Fig. 2a), resulting in a robust negative correlation ($r \approx -0.84$). This relationship also exhibits a clear scaling behavior, with an empirical sensitivity of approximately -0.096 Pg C yr^{-1} per unit Niño3.4 index (Figs. S11-S12). Both the GOBMs and MOM6 reproduce the historical SST–carbon relationship and the anomalously weak carbon response observed in 2023 (Fig. 2a).

To diagnose the processes governing the weak reduction of CO_2 outgassing during the 2023 El Niño, we next employ the MOM6 simulation for process attribution. Despite being a single-model framework, MOM6 reproduces the observed spatial patterns and magnitudes of

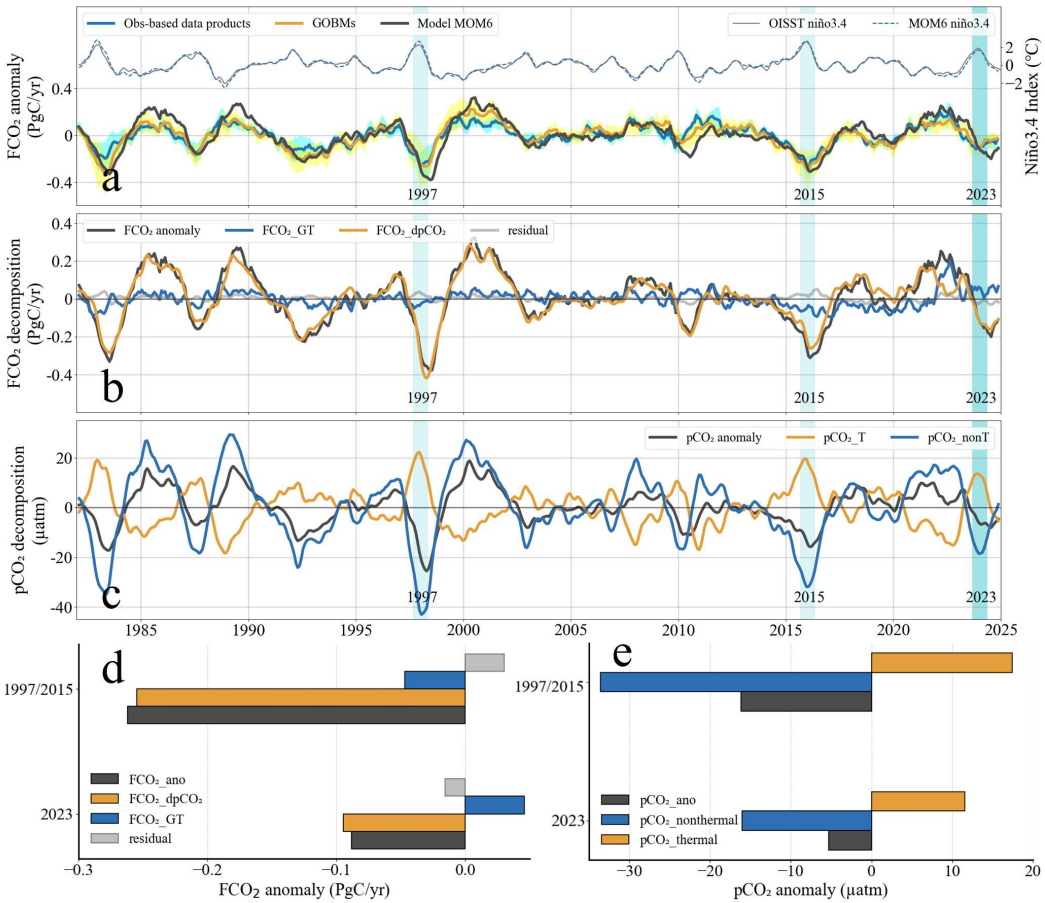


Fig. 2. Time series of tropical Pacific air–sea CO_2 flux anomalies and process decompositions during 1980–2024. (a) Air–sea CO_2 flux anomaly and Niño3.4 index. (b and d) Decomposition of FCO_2 into contributions from ΔpCO_2 (FCO_2–ΔpCO_2) and gas-transfer velocity (FCO_2–GT) following Eq. 1. (c and e) Decomposition of ocean pCO_2 into thermal (T) and non-thermal (nonT) components based on Eq. 2. Panels (d) and (e) show DJF mean contributions for the 1997/2015 extreme events and the 2023 event. CO_2 flux anomalies and its decompositions are area-integrated over the tropical Pacific (160°E–285°E, 10°S–10°N). Panel (a) includes nine observation-based fCO_2 products and ten GOBMs; shaded regions indicate ±1 standard deviation across models (blue) and data products (yellow). All other data are derived from MOM6–COBALT2.

carbon flux anomalies across both historical extreme El Niño events and the 2023 event (Figs. 1, 2a, and S1-S9), providing confidence in its ability to isolate the mechanisms responsible for the weakened carbon response. We therefore decompose the air–sea CO_2 flux anomaly (Eq. 1) into contributions from changes in the air–sea pCO_2 difference (FCO_2–ΔpCO_2), the gas-transfer velocity (FCO_2–GT; Eq. 1; Fig. 2b and 2d), and the residual term.

During the extreme El Niño events of 1997 and 2015 (Fig. 2d), the CO_2 flux anomaly simulated by the MOM6 model reached (-0.262 Pg C yr^{-1}), dominated by term of the air–sea ΔpCO_2 difference (-0.255 Pg C yr^{-1}), while concurrent reductions in gas-transfer velocity term (-0.05 Pg C yr^{-1}), associated with weakened trade winds, were small but acted in the same direction and reinforced the net flux decrease. In contrast, the simulated

CO_2 flux anomaly (-0.09 Pg C yr^{-1}) in 2023 El Niño (Fig. 2d) was driven by substantially weaker negative ΔpCO_2 anomalies (-0.1 Pg C yr^{-1}) and by an anomalously positive gas-transfer contribution in the same order of magnitude (0.05 Pg C yr^{-1}). The remaining flux anomaly in 2023 is explained by the nonlinear residual term. The 2023 El Niño was distinguished by an unusually weak air–sea pCO_2 response and a reversal of the gas-transfer contribution.

The air–sea pCO_2 difference (Fig. S15) is dominated by changes in oceanic pCO_2, with atmospheric pCO_2 contributing only about 1% of the variance across most El Niño events, including 2023. A subsequent decomposition of oceanic pCO_2 anomalies (Eq. 2) shows that (Fig. 2c and 22e), during previous extreme El Niño events, oceanic pCO_2 decreased by approximately 16.2 μatm, which was dominated by large non-thermal contributions (-33.6 μatm), partially offset by thermal contributions (17.4 μatm). In contrast, the ocean pCO_2 reduction in 2023 El Niño is only -5.4 uatm, which is driven by a disproportionately weakened non-thermal contribution (-16.0 μatm), while the thermal contribution remains comparatively strong (11.6 μatm). The thermal-to-nonthermal ratio increased from 0.52 (abs(17.4/-33.6)) in 1997/2015 to 0.73 (abs(11.6/-16)) in 2023, indicating that the non-thermal term was disproportionately weakened, while the thermal term remained relatively strong, resulting in a much smaller net reduction in oceanic pCO_2 during the 2023 El Niño.

3.3 Weakened Vertical Transport Controls the 2023 Carbon Response

The weak air–sea CO_2 flux anomalies during 2023 El Niño was distinguished by an unusually weak non-thermal oceanic pCO_2 response, a comparatively strong thermal pCO_2 contribution, and a reversed gas-transfer effect. The mechanisms underlying the weakened non-thermal response are examined through a temporal decomposition of the driving processes (Fig. 3, see Eq. 3 and Section S3 of the Supplementary Information for details of the decomposition).

During canonical extreme El Niño events (1997/2015), reductions in oceanic pCO_2 in the equatorial Pacific are driven predominantly by weakened vertical transport (V_{circ}), which reduces the entrainment of carbon-rich subsurface waters. Further, enhanced precipitation acts as a secondary contribution through dilution effect (Fig. 3d and 3h). This equatorial pCO_2 signal forms a coherent band extending from the central to the eastern Pacific and is subsequently redistributed poleward by horizontal (meridional) transport (H_{circ}), giving rise to spatially coherent, basin-scale reductions in oceanic pCO_2 across the tropical Pacific (Fig. 3b and 3f). Biological processes partially offset the vertically driven pCO_2 reduction through weakened biological carbon uptake, while the thermal contribution also provides a partial compensation relative to the dominant circulation-driven signal (Fig. 3 and S19).

The 2023 El Niño exhibits a distinctly altered process balance in the non-thermal oceanic pCO_2 budget relative to previous extreme El Niño events (Fig. 3). Unlike canonical El Niño responses, the vertical transport term fails to produce a continuous band of negative ocean pCO_2 anomalies along the equator, indicating that the suppression of equatorial upwelling and the entrainment of carbon-rich subsurface waters were spatially limited and dynamically inefficient in 2023 (Fig. 3c). Enhanced precipitation (FW) continues to locally

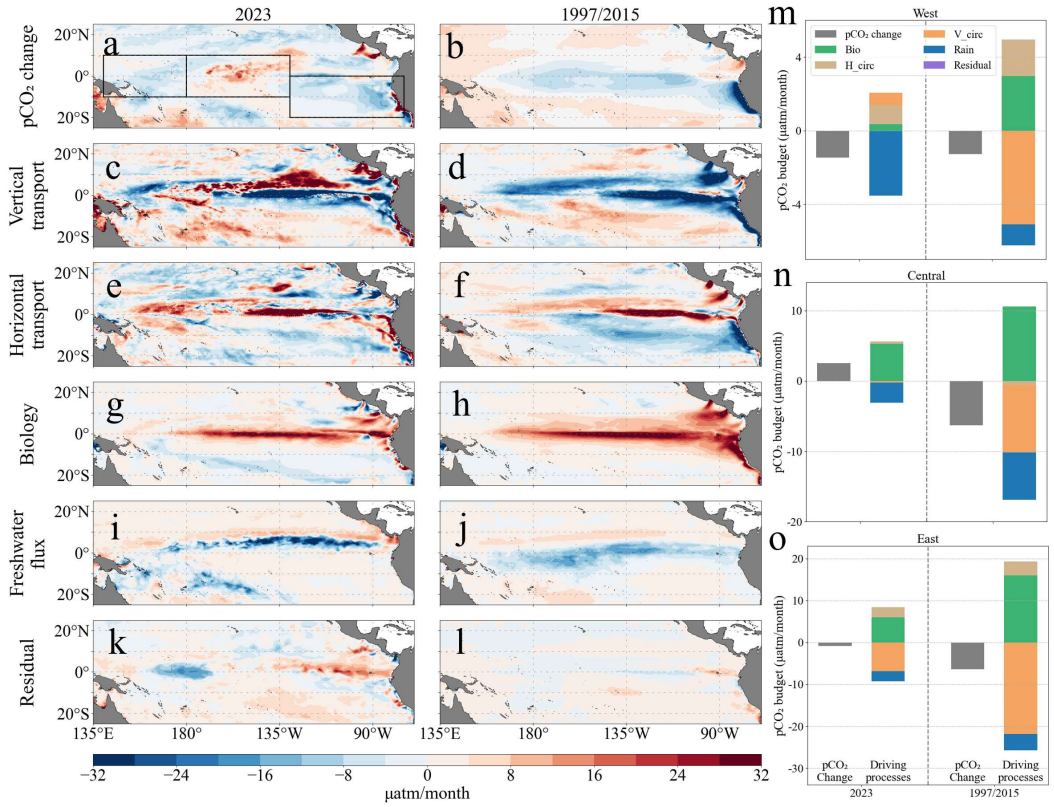


Fig. 3. Non-thermal ocean pCO_2 anomaly budget in the tropical Pacific during the 2023 El Niño and comparable extreme events (1997/2015). (a, b) Spatial distribution of total non-thermal pCO_2 change for 2023 and 1997/2015, respectively. (c–n) Contributions of individual processes to pCO_2 variability. (o–q) Regional pCO_2 budget comparisons between 2023 and 1997/2015 for the western, central, and eastern tropical Pacific, as indicated in (a). The western basin is defined as 140°E–180°E, 10°S–10°N), the central basin as 180°W–130°W, 10°S–10°N), and the eastern basin as 130°W–70°W, 20°S–0°N). All anomalies are computed as the December–February mean of monthly anomalies from MOM6-COBALT2.

reduce ocean pCO_2 along the equator (Fig. 3g); however, this signal is spatially discontinuous and displaced westward relative to that observed during earlier extreme El Niño events.

As a consequence of the reduced equatorial source signal, horizontal transport plays a diminished role in shaping the basin-scale pCO_2 variability in 2023. Rather than exporting a strong, coherent equatorial anomaly into the subtropics (15°N–15°S) as in previous extreme events, meridional transport redistributes weak and spatially patchy anomalies, confining their influence to the near-equatorial Pacific (10°N–10°S; Fig. 3e). Biological contributions are also reduced in both magnitude and spatial coherence relative to earlier extreme El Niño events (Fig. 3i), reflecting weaker modulation of surface DIC by biological uptake and remineralization. In contrast, the thermal contribution remains comparable in magnitude to that of previous events (Fig. S19), indicating that SST effects exert a stronger relative compensation in 2023 owing to the marked reduction in non-thermal controls, thereby partly contributing to the anomalously weak surface pCO_2 response.

We next examine the drivers of the weak 2023 CO_2 response by subdividing the tropical Pacific into western, central, and eastern regions. In the western tropical Pacific (Fig. 3m), the 2023 oceanic pCO_2 tendency (-1.05 μatm month^{-1}) is substantially stronger than canonical extreme El Niño events (-0.78 μatm month^{-1}), indicating a westward displacement of the anomalous carbon response relative to typical El Niño conditions. This regional signal is primarily driven by enhanced precipitation-induced dilution (-3.52 μatm month^{-1}, Fig. 3m). In contrast to previous extreme El Niño events, the vertical transport contribution in the western tropical Pacific becomes positive in 2023 (0.67 μatm month^{-1}), indicating that equatorial upwelling remains comparable to climatological conditions rather than being strongly suppressed during canonical extreme events.

The central tropical Pacific (Fig. 3n) exhibits the most pronounced departure from the canonical ENSO response and emerges as the primary contributor to the muted basin-scale carbon anomaly in 2023. In this region, the net ocean pCO_2 tendency (1.98 μatm month^{-1}) becomes positive, indicating an overall increase in pCO_2, in contrast to the canonical ENSO carbon response in which oceanic pCO_2 is reduced (-7.63 μatm month^{-1}). Precipitation (-2.92 μatm month^{-1}) and vertical transport (-0.20 μatm month^{-1}) provide the only negative contribution, whereas horizontal transport (0.37 μatm month^{-1}) and biological processes (5.28 μatm month^{-1}) all act to increase ocean pCO_2. This reversal sign of the net pCO_2 tendency relative to previous extreme El Niño events directly weakens the equatorial source of negative pCO_2 anomalies and represents the dominant mechanism underlying the muted tropical Pacific carbon response in 2023.

In the eastern tropical Pacific (Fig. 3o), ocean pCO_2 tendencies retain the same sign structure as during earlier extreme El Niño events but are uniformly reduced in magnitude (-3.85 vs -8.09 μatm month^{-1}). The variability remains primarily controlled by the vertical transport (-6.85 vs -21.82 μatm month^{-1}) and rainfall-related freshwater terms (-2.43 vs -3.92 μatm month^{-1}). Importantly, both the positive and negative non-thermal contributions are weakened by a similar proportion in 2023, preserving a broadly consistent balance among the individual processes despite the overall reduction in magnitude. This coherent scaling across all non-thermal components largely explains the reduced amplitude of the ocean pCO_2 response in this region.

3.4 Weak atmospheric and upper-ocean dynamical responses during the 2023 El Niño

The 2023 El Niño was characterized by strong oceanic warming that was only weakly coupled to the atmospheric circulation anomalies (Peng et al., 2025; Geng et al., 2024; Lian et al., 2023b). Despite elevated SSTs (Fig. 1), concurrent warming in the Atlantic and Indian Oceans weakened the Walker circulation and constrained the Bjerknes feedback (Peng et al., 2025), resulting in muted easterly trade winds (Fig. 4d-f), limited thermocline deepening, and only modest suppression of equatorial upwelling (Fig. 4g-l), together with enhanced but westward-displaced equatorial precipitation (Fig. 4a-c). While these forcings act in the canonical direction to suppress ocean pCO_2 through reduced upwelling and freshwater dilution, their magnitude and spatial structure differ substantially from those observed during the extreme El Niño events of 1997/2015.

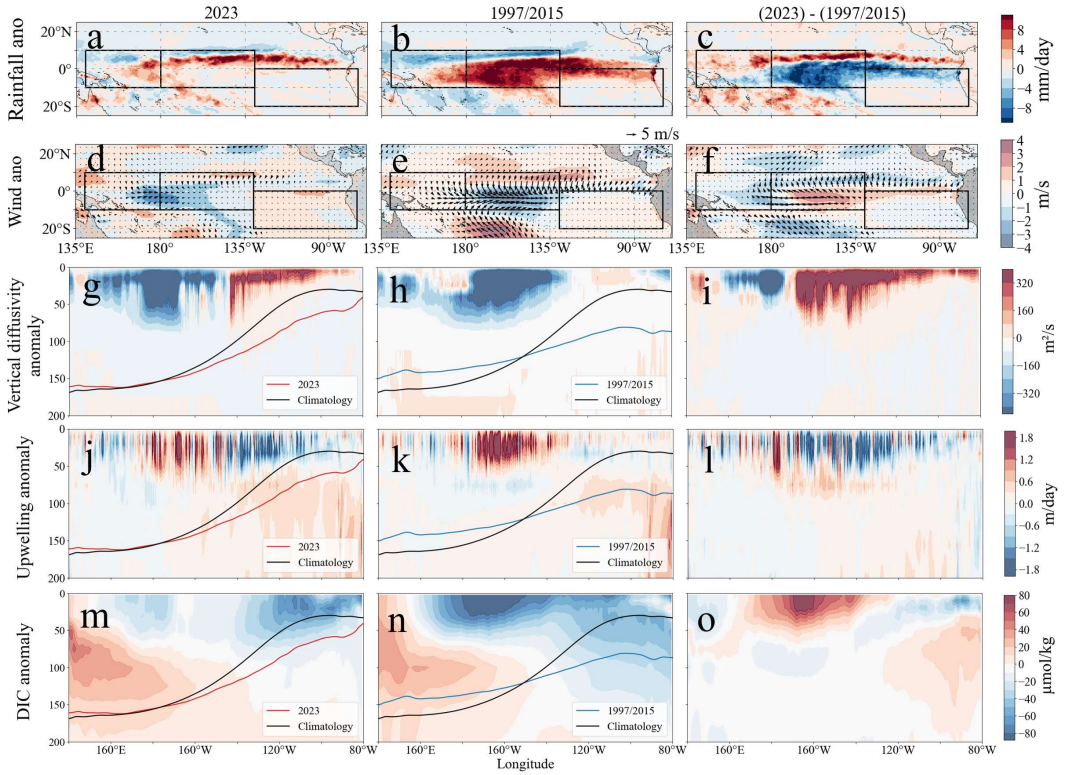


Fig. 4. Physical and biogeochemical forcing anomalies of the 2023 El Niño compared with the 1997/2015 extreme events, and their difference (2023 minus the 1997/2015 composite mean). (a–c) Precipitation anomalies from ERA5. (d–f) Surface wind (vectors) and wind speed anomalies (shading) from ERA5. (g–i) Equatorial (5°N–5°S) vertical profiles of upwelling velocity anomalies (shading) with thermocline depth overlaid from MOM6-COBALT2. (j–l) Equatorial (5°N–5°S) vertical profiles of diffusivity anomalies with thermocline depth overlaid from MOM6-COBALT2. (m–o) Equatorial (5°N–5°S) DIC anomaly profiles from MOM6-COBALT2. All anomalies are computed as the DJF mean of monthly anomalies.

During the 2023 El Niño, equatorial precipitation increases (6 mm/day) relative to climatology but is displaced westward (centered near 160°E) compared with previous extreme events (12 mm/day, centered near 220°E). This westward shift concentrates freshwater-driven dilution of DIC and oceanic pCO_2 in the western equatorial Pacific, while substantially weakening its influence in the central and eastern basins where ENSO-related carbon anomalies are typically strongest. Both observed and modeled SSS confirm weaker precipitation forcing in 2023 relative to 1997/2015 (Fig. S9). The diminished freshening anomaly indicates a reduced freshwater dilution effect on surface DIC, constraining the decrease in oceanic pCO_2 and thereby weakening outgassing suppression. As a result, freshwater forcing fails to generate a coherent basin-scale tropical oceanic pCO_2 signal.

Although easterly trade-wind weakening is evident during the 2023 El Niño, both the magnitude (-1.5 m s^{-1}) and zonal extent (155–210°E) of the wind anomalies are substantially smaller than the extreme events (-4.0 m s^{-1} and 155–230°E) of 1997/2015, particularly over the central and eastern equatorial Pacific. Consistent with the weaker wind forc-

ing, equatorially trapped wave activity—represented by sea surface height (SSH) anomalies (Fig. S16)—is also markedly reduced (0.08 m) in 2023 relative to the 1997/2015 extremes (0.24 m). The combined weakening of wind stress and wave-driven adjustment limits the thermocline deepening in 2023 (Fig. 4g-h), leaving the thermocline relatively shallow in the eastern basin(100-40 m in 2023 versus 120-55 m in 1997/2015).

One more influence of this relatively modest wind response is insufficient to strongly suppress equatorial upwelling and wind-driven vertical mixing (Fig. 4g-l). Fig. 4g-i shows that equatorial upwelling at subsurface depths (approximately 50–100 m) is only weakly suppressed in 2023 (-0.8 m/day), remaining much stronger than during the near shutdown observed in the extreme El Niño events of 1997/2015 (1.6 m/day). Above the thermocline, vertical mixing is weaker than climatology of 2023 (-600 m^2 s^{-1}) but remains substantially stronger than during earlier extreme El Niño events (-900 m^2 s^{-1}). Limited thermocline deepening and only modest suppression of upwelling and mixing sustained vertical carbon and nutrient supply, simultaneously constraining the non-thermal pCO_2 drawdown and attenuating the chlorophyll response (Figs. 1c and S7, S8).

4 Discussion and Summary

The 2023 El Niño marks a basin-scale departure from the canonical relationship between ENSO strength and tropical Pacific CO_2 outgassing, accompanied by similarly weak anomalies in chlorophyll and salinity, indicating a coherent physical–biogeochemical adjustment during the event. In 2023, the non-thermal pCO_2 anomaly was substantially weaker due to muted dynamical forcing, while the thermal anomaly remained comparable in magnitude. This shift enhanced the relative compensating effect of warming and diminished the net ocean pCO_2 anomaly.

Moreover, the gas-transfer contribution, which was negative and reinforced outgassing suppression during 1997/2015, became positive in 2023 and offset the already weak signal. The weak non-thermal response in 2023 reflects reduced dynamical perturbations in the ocean–atmosphere system. The 2023 El Niño exhibited strong ocean warming but only weak atmospheric coupling. Wind anomalies were weak, resulting in limited thermocline deepening, weakly suppressed upwelling and mixing. Vertical DIC supply therefore remained active, limiting the non-thermal reduction of surface pCO_2.

While our analysis identifies a muted carbon response during the 2023 El Niño that is physically coherent and dynamically consistent, precise quantification of its spatial extent and magnitude remains limited by sparse carbon observations in the tropical Pacific (Fig. S1 and S4). During the peak phase of the event (September 2023 to April 2024), the only sustained in situ pCO_2 measurements were located near 190°E (TAO). This site (Fig. S4a) recorded a pronounced decline in ocean pCO_2, consistent with a westward displacement of the region of strongest pCO_2 reduction in 2023 found in this study. In contrast, direct pCO_2 observations are nearly absent across the whole central and eastern tropical Pacific, where our analysis indicates that the reduction in pCO_2 was comparatively weak.

However, additional independent lines of evidence support our analysis that the muted carbon response extended across the central and eastern tropical Pacific. Chlorophyll and salinity anomalies in 2023 were likewise only about half as large as those observed 1997/2015,

consistent with weaker dynamical suppression and reduced non-thermal carbon drawdown. Although only about half of the observation-based fCO_2 products clearly capture the muted basin-scale flux anomaly in 2023 (Figs. S11,S13), nearly all ocean biogeochemical models simulate a substantially weakened ENSO–carbon response (Figs. S12,S14). The convergence across models indicates that the muted response in 2023 represents a physically and biogeochemically consistent signal.

Notably, Müller et al. (2025) reported that CO_2 flux anomalies in the eastern equatorial Pacific in 2023 were broadly consistent with expectations based on SST anomalies, using four data products. Among these data products, three showed a muted response, whereas one exhibited a strong anomaly. Consequently, the ensemble mean did not reveal a clear weakening of the carbon response and was associated with large uncertainty. Part of this discrepancy may arise from the use of the final prediction year in Müller et al. (2025), which is often affected by a tail-end effect and tends to exhibit larger variability. In contrast, our study finds that the CO_2 flux anomalies were weaker than expected from historical SST–carbon scaling, based on a comprehensive synthesis of all available observation-based fCO_2 products and GOBMs. This discrepancy highlights the sensitivity of inferred carbon flux anomalies to data selection and underscores the uncertainty associated with sparse observational constraints in the tropical Pacific. This reflects the need for expanded and sustained carbon observations to better resolve spatial shifts in pCO_2 and air–sea CO_2 flux under ongoing climate change.

During the period from December 2023 to February 2024, the global ocean carbon sink (60°E–60°N) weakened by approximately 0.14 Pg C yr^{-1} relative to the expected uptake. Our estimates indicate that the tropical Pacific accounted for nearly half of this reduction, contributing approximately 0.08 Pg C yr^{-1}. Climate projections suggest that El Niño events resembling the 2023 episode may become more frequent under continued warming (Peng et al., 2025). Meanwhile, rising atmospheric CO_2 and long-term changes in stratification, thermocline depth, and carbonate chemistry are altering the sensitivity of ocean pCO_2 to thermal and non-thermal forcing. Under this evolving background state, the dominant forcing on tropical Pacific carbon flux may shift from upwelling-driven toward thermally driven processes (Liao et al., 2021; Vaittinada Ayar et al., 2022). If such a transition occurs, future El Niño events could exert a stronger suppressing effect on ocean carbon uptake, thereby increasing the likelihood of climate-driven reductions in the global ocean carbon sink. Together with concurrent weakening of terrestrial carbon sinks, these changes point toward a potentially strengthening climate–carbon feedback in a warming world.

Consistent with this transition, the dominant region of global air–sea CO_2 flux interannual variability may also shift away from the tropical Pacific. In 2023, the largest carbon anomalies occurred in the mid- to high-latitude North Pacific and North Atlantic, where marine heatwaves were pronounced (Müller et al., 2025). This contrasts with earlier estimates attributing 70% of global air–sea CO_2 variability to the tropical Pacific (Le Quéré et al., 2000). Such a redistribution implies that future variability may be increasingly governed by extratropical thermal extremes rather than tropical upwelling, potentially increasing uncertainty in carbon flux projections.

Despite substantial progress in understanding ENSO–carbon coupling, the anomalous 2023 El Niño highlights persistent uncertainties in the magnitude and spatial extent of air–sea CO_2 flux anomalies, the consistency among data products, and the potential shifts in dominant regions and controlling forcing under ongoing climate change. Resolving these uncertainties will require expanded and sustained observations of surface pCO_2, particularly across the tropical Pacific, together with continued improvements in process-resolving models. Such efforts are critical for robustly quantifying ENSO-related carbon variability and improving projections of future ocean carbon–climate feedbacks.

References

Adcroft, A., Anderson, W., Balaji, V., Blanton, C., Bushuk, M., Dufour, C. O., ... Zhang, R. (2019). The gfdl global ocean and sea ice model om4.0: Model description and simulation features. *Journal of Advances in Modeling Earth Systems*, *11*(10), 3167-3211. doi: 10.1029/2019MS001726

Arteaga, L. A., Rousseaux, C. S., Cetinić, I., & Bushinsky, S. (2026). Extreme 2016 el niño heatwave weakened carbon export and respiration in the equatorial pacific. *Communications Earth & Environment*. Retrieved from `https://doi.org/10.1038/s43247-026-03441-y` (Published online 30 March 2026) doi: 10.1038/s43247-026-03441-y

Bakker, D. C. E., Pfeil, B., Landa, C. S., Metzl, N., O'Brien, K. M., Olsen, A., ... Xu, S. (2016). A multi-decade record of high-quality fco_2 data in version 3 of the surface ocean co_2 atlas (socat). *Earth System Science Data*, *8*(2), 383–413. Retrieved from `https://essd.copernicus.org/articles/8/383/2016/` doi: 10.5194/essd-8-383-2016

Chau, T. T. T., Gehlen, M., & Chevallier, F. (2022). A seamless ensemble-based reconstruction of surface ocean pco2 and air–sea co2 fluxes over the global coastal and open oceans. *Biogeosciences*, *19*(4), 1087–1109. doi: 10.5194/bg-19-1087-2022

Cosca, C. E., Feely, R. A., Boutin, J., Etcheto, J., McPhaden, M. J., Chavez, F. P., & Strutton, P. G. (2003). Seasonal and interannual co2 fluxes for the central and eastern equatorial pacific ocean as determined from fco2–sst relationships. *Journal of Geophysical Research: Oceans*, *108*(C8).

DeVries, T., Yamamoto, K., Wanninkhof, R., Gruber, N., Hauck, J., Müller, J. D., ... Zeng, J. (2023). Magnitude, trends, and variability of the global ocean carbon sink from 1985 to 2018. *Global Biogeochemical Cycles*, *37*(10), e2023GB007780. Retrieved from `https://agupubs.onlinelibrary.wiley.com/doi/abs/10.1029/2023GB007780` (e2023GB007780 2023GB007780) doi: https://doi.org/10.1029/2023GB007780

Doney, S. C., Lima, I., Feely, R. A., Glover, D. M., Lindsay, K., Mahowald, N., ... Wanninkhof, R. (2009). Mechanisms governing interannual variability in upper-ocean inorganic carbon system and air–sea co2 fluxes: Physical climate and atmospheric dust. *Deep Sea Research Part II: Topical Studies in Oceanography*, *56*(8), 640–655. Retrieved from `https://doi.org/10.1016/j.dsr2.2008.12.006` doi: 10.1016/j.dsr2.2008.12.006

Dong, F., Li, Y., & Wang, B. (2017). Assessment of responses of tropical pacific air–sea co2 flux to enso in 14 cmip5 models. *Journal of Climate*, *30*(21), 8595–8613. Retrieved from `https://doi.org/10.1175/JCLI-D-16-0543.1` doi: 10.1175/JCLI-D-16-0543.1

Fan, H., Lin, S., Zhang, L., Deng, K., Luo, H., Xie, M., ... Wang, C. (2026). Multi-year la niña dampens the southern oscillation during subsequent el niño through tropical

pacific-rooted dynamics. *The Innovation Geoscience*, 100224. Retrieved from https://www.the-innovation.org/geoscience/article/id/69dc716ba26741285585aea7 doi: 10.59717/j.xinn-geo.2026.100224

Feely, R. A., Boutin, J., Cosca, C. E., Dandonneau, Y., Etcheto, J., Inoue, H. Y., ... Wanninkhof, R. (2002). Seasonal and interannual variability of co_2 in the equatorial pacific. *Deep Sea Research Part II: Topical Studies in Oceanography*, *49*(13), 2443–2469. (The Equatorial Pacific JGOFS Synthesis) doi: 10.1016/S0967-0645(02)00044-9

Feely, R. A., Takahashi, T., Wanninkhof, R., McPhaden, M. J., Cosca, C. E., Sutherland, S. C., & Carr, M.-E. (2006). Decadal variability of the air-sea co2 fluxes in the equatorial pacific ocean. *Journal of Geophysical Research: Oceans*, *111*(C8). Retrieved from https://agupubs.onlinelibrary.wiley.com/doi/abs/10.1029/2005JC003129 doi: https://doi.org/10.1029/2005JC003129

Friedlingstein, P., O'Sullivan, M., Jones, M. W., Andrew, R. M., Bakker, D. C. E., Hauck, J., ... Zeng, J. (2025). Global carbon budget 2025. *Earth System Science Data Discussions*, *2025*, 1–139. Retrieved from https://essd.copernicus.org/preprints/essd-2025-659/ doi: 10.5194/essd-2025-659

Friedlingstein, P., O'Sullivan, M., Jones, M. W., Andrew, R. M., Hauck, J., Landschützer, P., ... Zeng, J. (2025). Global carbon budget 2024. *Earth System Science Data*, *17*(3), 965–1039. doi: 10.5194/essd-17-965-2025

Geng, X., Kug, J.-S., Shin, N.-Y., Zhang, W., & Chen, H.-C. (2024). On the spatial double peak of the 2023–2024 el niño event. *Communications Earth & Environment*, *5*(1), 691. doi: 10.1038/s43247-024-01870-1

Gregor, L., & Gruber, N. (2021). Oceansoda-ethz: a global gridded data set of the surface ocean carbonate system for seasonal to decadal studies of ocean acidification. *Earth System Science Data*, *13*(2), 777–808. Retrieved from https://essd.copernicus.org/articles/13/777/2021/ doi: 10.5194/essd-13-777-2021

Gruber, N., Bakker, D. C. E., DeVries, T., Gregor, L., Hauck, J., Landschützer, P., ... Müller, J. D. (2023). Trends and variability in the ocean carbon sink. *Nature Reviews Earth & Environment*, *4*(2), 119–134. doi: 10.1038/s43017-022-00381-x

Hauck, J., Landschützer, P., Sreeush, M., & Roobaert, A. (2025). *Global carbon budget 2025, surface ocean fugacity of co_2 (fco_2) and air–sea co_2 flux of individual global ocean biogeochemical models and surface ocean fco_2-based data-products.* Data set, Zenodo. Retrieved from https://doi.org/10.5281/zenodo.17579108 doi: 10.5281/zenodo.17579108

Hauck, J., Nissen, C., Landschützer, P., Rödenbeck, C., Bushinsky, S., & Olsen, A. (2023, 05). Sparse observations induce large biases in estimates of the global ocean co2 sink: an ocean model subsampling experiment. *Philosophical Transactions of the Royal Society A: Mathematical, Physical and Engineering Sciences*, *381*(2249), 20220063. Retrieved from https://doi.org/10.1098/rsta.2022.0063 doi: 10.1098/rsta.2022.0063

Hu, R., Lian, T., Liu, T., Wang, J., Song, X., Chen, H., & Chen, D. (2024). Predicting the 2023/24 el niño from a multi-scale and global perspective. *Communications Earth & Environment*, *5*, 675. doi: 10.1038/s43247-024-01867-w

Ishii, M., Carter, B. R., Toyama, K., Rodgers, K. B., Feely, R. A., Chau, T.-T.-T., ... Tsujino, H. (2025). Co2 uptake in the pacific from 1985 to 2018: A comparative assessment of observation- and model-based estimates. *Global Biogeochemical Cycles*, *39*(5), e2024GB008355. Retrieved from https://agupubs.onlinelibrary.wiley.com/doi/

abs/10.1029/2024GB008355 (e2024GB008355 2024GB008355) doi: https://doi.org/10.1029/2024GB008355

Jones, C. D., Collins, M., Cox, P. M., & Spall, S. A. (2001). The carbon cycle response to enso: A coupled climate–carbon cycle model study. *Journal of Climate*, *14*(21), 4113–4129. doi: 10.1175/1520-0442(2001)014⟨4113:TCCRTE⟩2.0.CO;2

Kim, J.-W., Tian, B., & Yu, J.-Y. (2024). Unusual and persistent easterlies restrained the 2023/24 el niño development after a triple-dip la niña. *npj Climate and Atmospheric Science*, *7*, 198. doi: 10.1038/s41612-024-00890-0

Landschützer, P., Gruber, N., Bakker, D. C. E., & Schuster, U. (2014). Recent variability of the global ocean carbon sink. *Global Biogeochemical Cycles*, *28*(9), 927–949. doi: 10.1002/2014GB004853

Landschützer, P., Ilyina, T., & Lovenduski, N. S. (2019). Detecting regional modes of variability in observation-based surface ocean pco2. *Geophysical Research Letters*, *46*(5), 2670-2679. Retrieved from https://agupubs.onlinelibrary.wiley.com/doi/abs/10.1029/2018GL081756 doi: https://doi.org/10.1029/2018GL081756

Le Quéré, C., Orr, J. C., Monfray, P., Aumont, O., & Madec, G. (2000). Interannual variability of the oceanic sink of co2 from 1979 through 1997. *Global Biogeochemical Cycles*, *14*(4), 1247-1265. Retrieved from https://agupubs.onlinelibrary.wiley.com/doi/abs/10.1029/1999GB900049 doi: https://doi.org/10.1029/1999GB900049

Li, Y., Jing, Y., & Xu, Y. (2024). Weak interannual variability of sea–air carbon flux in the tropical pacific ocean simulated by cmip6 models. *Ocean Modelling*, *187*, 102300. Retrieved from https://www.sciencedirect.com/science/article/pii/S1463500323001403 doi: https://doi.org/10.1016/j.ocemod.2023.102300

Lian, T., Wang, J., Chen, D., Liu, T., & Wang, D. (2023a). A strong 2023/24 el niño is staged by tropical pacific ocean heat content buildup. *Ocean-Land-Atmosphere Research*, *2*, 0011. Retrieved from https://spj.science.org/doi/abs/10.34133/olar.0011 doi: 10.34133/olar.0011

Lian, T., Wang, J., Chen, D., Liu, T., & Wang, D. (2023b, 05). A strong 2023/24 el niño is staged by tropical pacific ocean heat content buildup. *Ocean-Land-Atmosphere Research*, *2*. doi: 10.34133/olar.0011

Liao, E., Resplandy, L., Liu, J., & Bowman, K. W. (2020). Amplification of the ocean carbon sink during el niños: Role of poleward ekman transport and influence on atmospheric co2. *Global Biogeochemical Cycles*, *34*(9), e2020GB006574. Retrieved from https://agupubs.onlinelibrary.wiley.com/doi/abs/10.1029/2020GB006574 (e2020GB006574 2020GB006574) doi: https://doi.org/10.1029/2020GB006574

Liao, E., Resplandy, L., Liu, J., & Bowman, K. W. (2021). Future weakening of the enso ocean carbon buffer under anthropogenic forcing. *Geophysical Research Letters*, *48*(18), e2021GL094021. Retrieved from https://agupubs.onlinelibrary.wiley.com/doi/abs/10.1029/2021GL094021 (e2021GL094021 2021GL094021) doi: https://doi.org/10.1029/2021GL094021

Mayot, N., Buitenhuis, E. T., Wright, R. M., Hauck, J., Bakker, D. C. E., & Le Quéré, C. (2024). Constraining the trend in the ocean co2 sink during 2000–2022. *Nature Communications*, *15*(1), 8429. doi: 10.1038/s41467-024-52641-7

McKinley, G. A., Follows, M. J., & Marshall, J. (2004). Mechanisms of air-sea co2

flux variability in the equatorial pacific and the north atlantic. *Global Biogeochemical Cycles*, *18*(2). Retrieved from https://doi.org/10.1029/2003GB002179 doi: 10.1029/2003GB002179

Müller, J. D., Gruber, N., Schneuwly, A., Bakker, D. C. E., Gehlen, M., Gregor, L., ... McKinley, G. A. (2025). Unexpected decline in the ocean carbon sink under record-high sea surface temperatures in 2023. *Nature Climate Change*, *15*, 978–985. Retrieved from https://doi.org/10.1038/s41558-025-02380-4 doi: 10.1038/s41558-025-02380-4

Parc, L., Bellenger, H., Bopp, L., Perrot, X., & Ho, D. T. (2024). Global ocean carbon uptake enhanced by rainfall. *Nature Geoscience*, *17*(9), 851–857. doi: 10.1038/s41561-024-01517-y

Peng, Q., Xie, S.-P., Miyamoto, A., Deser, C., Zhang, P., & Luongo, M. T. (2025). Strong 2023–2024 El Niño generated by ocean dynamics. *Nature Geoscience*, *18*, 471–478. Retrieved from https://doi.org/10.1038/s41561-025-01700-9 doi: 10.1038/s41561-025-01700-9

Ran, Q., Zhang-gui, W., Zhi, C., Shi-ming, L., Yan-hong, Y., & Hong-gang, L. (2005). Distribution of marine carbon dioxide and its relationship with other marine parameters and air-sea anomalies. *Acta Oceanologica Sinica (In Chinese with English abstract)*, *27*(6), 30–37.

Roobaert, A., Resplandy, L., Laruelle, G. G., Liao, E., & Regnier, P. (2022). A framework to evaluate and elucidate the driving mechanisms of coastal sea surface pCO_2 seasonality using an ocean general circulation model (mom6-cobalt). *Ocean Science*, *18*(1), 67–88. Retrieved from https://os.copernicus.org/articles/18/67/2022/ doi: 10.5194/os-18-67-2022

Stock, C. A., Dunne, J. P., Fan, S., Ginoux, P., John, J., Krasting, J. P., ... Zadeh, N. (2020). Ocean biogeochemistry in gfdl's earth system model 4.1 and its response to increasing atmospheric co2. *Journal of Advances in Modeling Earth Systems*, *12*(10), e2019MS002043. doi: 10.1029/2019MS002043

Sun, C., Liao, E., & Zhu, X. (2025). Asymmetrical ocean carbon responses in the tropical pacific ocean to la niña and el niño. *Geophysical Research Letters*, *52*(4), e2024GL112039. Retrieved from https://agupubs.onlinelibrary.wiley.com/doi/abs/10.1029/2024GL112039 (e2024GL112039 2024GL112039) doi: https://doi.org/10.1029/2024GL112039

Sun, Q., & Du, Y. (2025). Impact of sst and ocean dynamics on the interannual variability of air-sea co2 fluxes in the tropical pacific. *Climate Dynamics*, *63*. Retrieved from https://api.semanticscholar.org/CorpusID:275977277

Sutton, A. J., Feely, R. A., Sabine, C. L., McPhaden, M. J., Takahashi, T., Chavez, F. P., ... Mathis, J. T. (2014). Natural variability and anthropogenic change in equatorial pacific surface ocean pco2 and ph. *Global Biogeochemical Cycles*, *28*(2), 131-145. Retrieved from https://agupubs.onlinelibrary.wiley.com/doi/abs/10.1002/2013GB004679 doi: https://doi.org/10.1002/2013GB004679

Takahashi, T., Olafsson, J., Goddard, J. G., Chipman, D. W., & Sutherland, S. C. (1993). Seasonal variation of co2 and nutrients in the high-latitude surface oceans: A comparative study. *Global Biogeochemical Cycles*, *7*(4), 843-878. doi: 10.1029/93GB02263

Turk, D., Zappa, C. J., Meinen, C. S., Christian, J. R., Ho, D. T., Dickson, A. G., & McGillis, W. R. (2010). Rain impacts on co_2 exchange in the western equatorial pacific

ocean. *Geophysical Research Letters*, *37*(23). doi: 10.1029/2010GL045520

Vaittinada Ayar, P., Bopp, L., Christian, J. R., Ilyina, T., Krasting, J. P., Séférian, R., ... Tjiputra, J. (2022). Contrasting projections of the enso-driven co_2 flux variability in the equatorial pacific under high-warming scenario. *Earth System Dynamics*, *13*(3), 1097–1118. Retrieved from https://esd.copernicus.org/articles/13/1097/2022/ doi: 10.5194/esd-13-1097-2022

Wang, X., Murtugudde, R., Hackert, E., Wang, J., & Beauchamp, J. (2015). Seasonal to decadal variations of sea surface pco2 and sea-air co2 flux in the equatorial oceans over 1984–2013: A basin-scale comparison of the pacific and atlantic oceans. *Global Biogeochemical Cycles*, *29*(5), 597-609. Retrieved from https://agupubs.onlinelibrary.wiley.com/doi/abs/10.1002/2014GB005031 doi: https://doi.org/10.1002/2014GB005031

Watanabe, M., Tatebe, H., Koyama, H., Hajima, T., Watanabe, M., & Kawamiya, M. (2020). Importance of el niño reproducibility for reconstructing historical co_2 flux variations in the equatorial pacific. *Ocean Science*, *16*(6), 1431–1442. Retrieved from https://os.copernicus.org/articles/16/1431/2020/ doi: 10.5194/os-16-1431-2020

Wong, S. C. K., McKinley, G. A., & Seager, R. (2022). Equatorial pacific pco2 interannual variability in cmip6 models. *Journal of Geophysical Research: Biogeosciences*, *127*(12), e2022JG007243. Retrieved from https://agupubs.onlinelibrary.wiley.com/doi/abs/10.1029/2022JG007243 (e2022JG007243 2022JG007243) doi: https://doi.org/10.1029/2022JG007243

Xiu, P., & Chai, F. (2014). Variability of oceanic carbon cycle in the north pacific from seasonal to decadal scales. *Journal of Geophysical Research: Oceans*, *119*(8), 5270-5288. Retrieved from https://agupubs.onlinelibrary.wiley.com/doi/abs/10.1002/2013JC009505 doi: https://doi.org/10.1002/2013JC009505

Yang, C., & Li, T. (2025). Easterly anomalies during el niño in january 2024: What caused the "decoupling"? *Journal of Climate*, *38*(23), 7217 - 7228. Retrieved from https://journals.ametsoc.org/view/journals/clim/38/23/JCLI-D-24-0689.1.xml doi: 10.1175/JCLI-D-24-0689.1

Zhang, L., & Liao, E. (2025). Unprecedented carbon accumulation in the indian ocean during 2016–2017. *Geophysical Research Letters*, *52*(20), e2025GL117199. Retrieved from https://agupubs.onlinelibrary.wiley.com/doi/abs/10.1029/2025GL117199 (e2025GL117199 2025GL117199) doi: https://doi.org/10.1029/2025GL117199

Zhang, M., Zhu, X., & Ji, X. (2025). The intraseasonal oscillation of pco2 over the southeast coast of vietnam in boreal summer. *Environmental Research Communications*, *7*(5), 055028. doi: 10.1088/2515-7620/add990

Supplementary Files

This is a list of supplementary files associated with this preprint. Click to download.

- si2.pdf
- supp.pdf
- supp.pdf
- supp.pdf